frontiers in Materials

ORIGINAL RESEARCH
published: 30 June 2016
doi: 10.3389/fmats.2016.00031

Role of Surfactant during Microemulsion Photopolymerization for the Creation of Three-Dimensional Liquid Crystal Elastomer Microsphere Spatial Cell Scaffolds

*Tanmay Bera[1], Christopher Malcuit[2], Robert J. Clements[2] and Elda Hegmann[1,2,3]**

[1] Chemical Physics Interdisciplinary Program, Liquid Crystal Institute, Kent State University, Kent, OH, USA, [2] Department of Biological Sciences, Kent State University, Kent, OH, USA, [3] Department of Chemistry and Biochemistry, Kent State University, Kent, OH, USA

Three-dimensional (3D) cell scaffolds based on nematic liquid crystal elastomer (LCE) microsphere architectures support the attachment and proliferation of C2C12 myoblasts, neuroblastomas (SHSY5Y), and human dermal fibroblasts (hDF). The microsphere spatial cell scaffolds were prepared by an oil-in-water microemulsion photopolymerization of reactive nematic mesogens in the presence of various surfactants, and the as-prepared scaffold constructs are composed of smooth surface microspheres with diameter ranging from 10 to 30 μm. We here investigate how the nature and type of surfactant used during the microemulsion photopolymerization impacts both the size and size distribution of the resulting microspheres and their surface morphology, i.e., the surface roughness.

Keywords: liquid crystal elastomer, 3D cell scaffold, microspheres, reactive mesogens, microemulsion photopolymerization, artificial muscle, cell proliferation

OPEN ACCESS

Edited by:
Anupam Sengupta, MIT, USA

Reviewed by:
Justin Lee Brown, Pennsylvania State University, USA
Stephanie Michelle Willerth, University of Victoria, Canada
Anindita Basu, Broad Institute, USA

****Correspondence:***
Elda Hegmann
ehegmann@kent.edu

Specialty section:
This article was submitted to Biomaterials, a section of the journal Frontiers in Materials

Received: *11 March 2016*
Accepted: *21 June 2016*
Published: *30 June 2016*

Citation:
Bera T, Malcuit C, Clements RJ and Hegmann E (2016) Role of Surfactant during Microemulsion Photopolymerization for the Creation of Three-Dimensional Liquid Crystal Elastomer Microsphere Spatial Cell Scaffolds. Front. Mater. 3:31. doi: 10.3389/fmats.2016.00031

INTRODUCTION

Numerous biological and biocompatible synthetic materials have been developed for specific applications in tissue regeneration, and most are based on proteins, polysaccharides, polymers (e.g., PEG), peptides, or ceramic scaffolds (Koegler and Griffith, 2004; Kotov et al., 2004; Liu et al., 2005; Shanbhag et al., 2005; Lee and Kotov, 2009; Lee et al., 2009; DeForest and Anseth, 2012; McCall et al., 2012; Alge et al., 2013; Lewis and Anseth, 2013; McKinnon et al., 2013). Any material that is designed for use in tissue regeneration, or cell studies in general, should promote adhesion, proliferation, and an environment for cell maturation. With the exception of some shape-memory polymers, only very few of these materials are examples of biocompatible scaffolds that can, by choice and on demand, respond to several external stimuli with an anisotropic molecular ordering event like liquid crystal elastomers (LCEs). LCEs are anisotropic rubbers with mesogenic molecular units in the main or side chain. Abbott et al. (2010) (Lockwood et al., 2006) and Fang et al. (2003) have provided significant evidence that liquid crystals (LCs) can sense the growth, orientational order, and differentiation of cells. In particular, Abbott reported that the orientational order of nematic LCs is coupled with the orientational order of cells *via* a thin layer of Matrigel® (Lockwood et al., 2006; Lowe and Abbott, 2012). Nematic LC molecules also align at cell surfaces; this alignment depends on the cell type, i.e., their shape. An important advantage of LCEs is their straightforward synthetic access including many structural variations and easily tunable elastic properties, often starting from inexpensive commercially available materials permitting scale-up and high reproducibility. Several reports

highlight that the contractile and expansion properties of these materials are associated with Young's moduli (measured by tensile tests) between tens of kilopascal to several megapascal, leading to the concept that LCEs can be regarded as artificial muscles or used as biologically or medically relevant actuators (Ratna et al., 2001; Thomsen et al., 2001; Finkelmann and Shahinpoor, 2002; Mayer and Zentel, 2002; Buguin et al., 2006; Li and Keller, 2006; Fleischmann and Zentel, 2013; Marshall et al., 2014; Pei et al., 2014). De Gennes (1997) first proposed the idea of nematic gels and LCEs as artificial muscles (De Gennes et al., 1997).

Muscle regeneration in the body is highly spatially and temporally regulated by the expression of muscle specific proteins [Chargè and Rudnicki, 2004; reviewed in Shi and Garry (2006) and Zammit et al. (2006)] and, most importantly, by interactions of cells with their microenvironment (Discher et al., 2009). For example, in skeletal muscles, adhesive ligands of the extracellular matrix (ECM) are critical for cell anchoring. In addition, physical properties of the ECM are responsible for the acquisition of the contractile phenotype. In addition, Discher et al. demonstrated that the elastic modulus of the substrate plays a key role in muscle differentiation (Engler et al., 2006; Gilbert et al., 2010).

We have previously reported the use of biocompatible smectic LCEs where their anisotropic nature and different internal morphology promoted not only cell adhesion and permeation within the bulk of LCEs (Sharma et al., 2014; Gao et al., 2016) but also a suitable substrate to support three-dimensional (3D) cell growth. We also reported (Bera et al., 2015) the use of microemulsion photopolymerization in a proof-of-concept study on the utilization of nematic LCEs as 3D connected microsphere scaffolds for muscle cells. In this particular work, cetyltrimethylammonium bromide (CTAB) was used as a surfactant for the microemulsion polymerization reaction (Vennes et al., 2005; Lange et al., 2007; Haseloh et al., 2010, 2011). The nematic LCE cell scaffold constructs created by this reaction were composed of LCE microspheres with faceted surfaces and significant interconnected space between them (i.e., these microspheres were not tightly packed). The overall porous architecture was suitable as 3D cell scaffold for smooth muscle cells, and allowed sufficient management of mass transport (i.e., nutrients, waste, and gases) as evident longitudinal cell studies. In this work, we are exploring the use of several other surfactants, including cationic, anionic, and non-ionic surfactants, some of which are less cytotoxic than CTAB, and study effects of these surfactants on the size and size distribution as well as the surface morphology of the resulting microsphere scaffolds. In addition, we are expanding the use of these nematic LCEs to other cell lines including neuroblastomas (SHSY5Y) and human dermal fibroblasts (hDF; a primary cell line).

MATERIALS AND METHODS

Materials

1,4-bis-[4-(6-acryloyloxyhexyloxy)benzoyloxy]-2-methylbenzene (cross-linker, CL) and 4-(heptyloxy)phenyl 4-((6-(acryloyloxy)hexyl)oxy)benzoate (monomer, M) were purchased from Synthon Chemicals GmbH (Germany). 2,2-dimethyoxy-2-phenylacetophenone (photoinitiator, PI), and surfactants sodium dodecyl sulfate (SDS, anionic surfactant), hexadecyltrimethylammonium bromide (CTAB, cationic surfactant), polyethylene glycol *p*-(1,1,3,3-tetra-methylbutyl)-phenyl ether (TritonX-100, non-ionic surfactant), polyethylene glycol hexadecyl ether (BrijC10, non-ionic surfactant), and 3-((3-cholamidopropyl) dimethylammonio)-1-propanesulfonate (CHAPS 100 mM solution, zwitterionic) were purchased from Sigma-Aldrich. Deionized water (DI, Millipore; resistivity 18.1 MΩ) and toluene (EMD Millipore grade, purified by a PureSolv solvent purification system, Innovative Technology, Inc.) and used as solvents.

Materials Characterization

Scanning electron microscopy (SEM) was performed using a Hitachi S-2600N; samples were sputter-coated with Pd–Au. Polarized optical microscopy (POM) was performed using an Olympus BX53 (bright field and crossed polarizers). Confocal microscopy was carried out using an Olympus FV1000; ImageJ (Rasband, 1997–2015) was used for image analysis/processing.

Elastomer Synthesis

We followed the synthetic procedure used for the preparation of the LCE microsphere scaffolds based on the standard photopolymerization reaction of acrylate-based, nematic phenylbenzoate LCEs previously reported in the literature (Harris et al., 2005; Lub et al., 2005). In short, the synthesis of the LC elastomer starts with accurately weighing monomer (86 wt.%), cross-linker (10 wt.%), and photoinitiator (4 wt.%) in a clean vial. All components were then dissolved in anhydrous toluene, followed by UV-induced photopolymerization reaction to obtain the LCEs. A typical synthesis will contain 69 mg of monomer, 8 mg of cross-linker, and 3 mg of photoinitiator dissolved into 100 μL of anhydrous toluene. This solution was added to water containing 10 vol.% of 10 mM aqueous surfactant solution. The volumes of the toluene solution and aqueous phase were adjusted to obtain various toluene/water proportions. We previously reported several toluene/water ratios (Bera et al., 2015) and showed that the amount of surfactant present in the mixture affects microsphere shape and porosity. Here, we selected the E20 formulation (80:20 toluene/water ratio, v:v), where 200 μL of toluene was added to a glass vial containing 700 μL of DI water and 100 μL of 10 mM aqueous surfactant (see **Scheme 1**). The mixture was then sonicated (40 kHz, 10 min) to form a milky-white toluene/water emulsion. The photopolymerization was initiated under 365 nm UV light irradiation for 15 min, followed by tightly sealing the vial and heating it to 50°C. The heating was continued for 12 h in a temperature-controlled sand bath, which completes the polymerization reaction. The washing and recovery of the elastomer samples remained the same ensuring that all unreacted monomers, cross-linker, and surfactant were completely removed. In the case of the stained elastomers, rhodamine was added to the elastomer synthesis mixture containing monomers, crosslinker, toluene, and PI (rhodamine was calculated at 0.1% of elastomer weight). The mixture containing the rhodamine dye was then exposed to UV to form the rhodamine-doped LCE.

Cell Cultures

Liquid crystal elastomer samples were seeded with murine C2C12 myoblast, neuroblastomas (SHSY5Y), and hDF from ATCC and

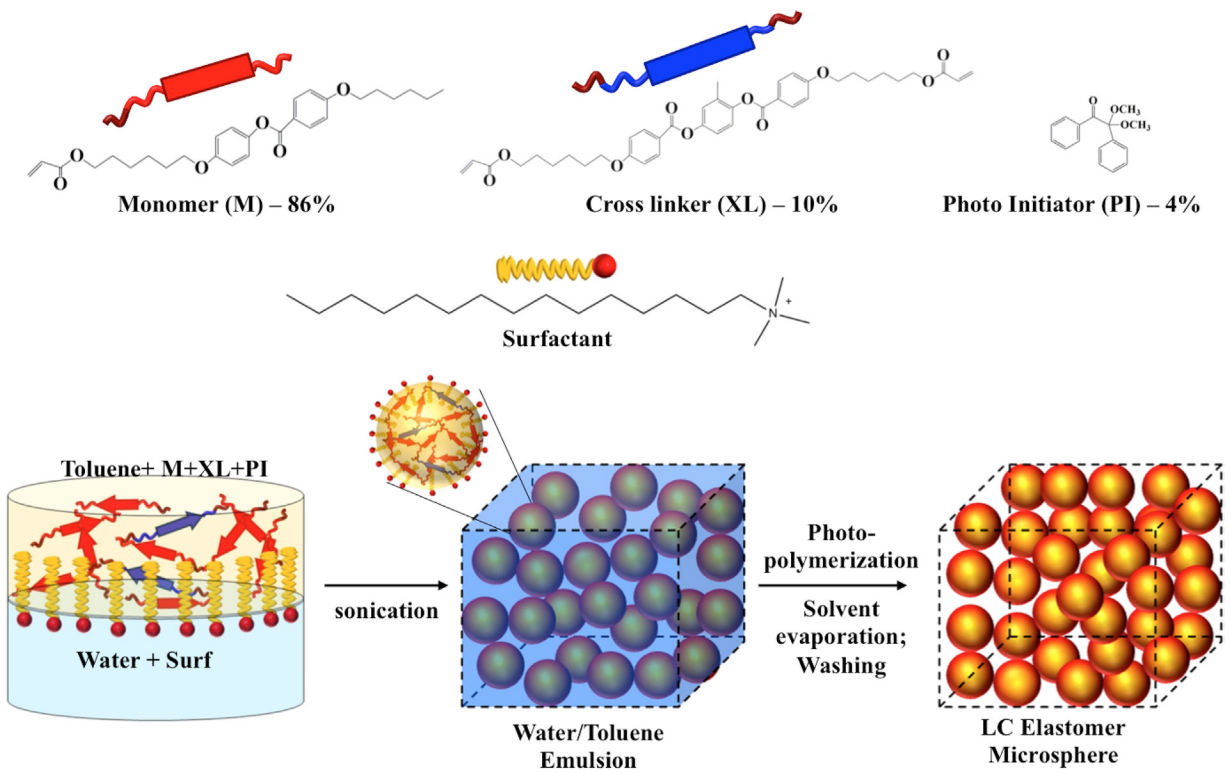

SCHEME 1 | **Synthetic pathway for the formation of globular LCEs**.

cultured using standard sterile techniques. Growth medium for C2C12 contained 90% Dulbecco's modified Eagle medium (DMEM), supplemented with 10% fetal bovine serum (FBS) and 1% Penicillin–Streptomycin. For the SHSY5Y, 50% of DMEM was supplemented with Ham F12 (i.e., 45% DMEM, 45% Ham F12, and 10% FBS). Prior to cell seeding, LCEs were washed with 70% ethanol, rinsed twice with phosphate-buffered saline (PBS), air dried under sterile conditions and UV-irradiated for 30 min. Then, they were treated with 1 wt.% poly-D-lysine solution for 2 h, rinsed with PBS, and placed carefully in 12-well cell culture plates. Approximately 5×10^4 C2C12 cells (passage 8) suspended in growth media were seeded onto each of the LCE samples. The LCEs along with the cells were incubated at 37°C with 5% CO_2 for about 6 h to promote cell adhesion, followed by addition of growth media. Medium was changed every 2 days. After 10 days, cells were fixed with 4% paraformaldehyde and stained with DAPI (1:2000, Life Technologies) to identify cell nuclei.

Cell–Elastomer Imaging

Fixed samples were imaged using confocal microscopy (Olympus FV1000). For 3D imaging, several images were sequentially taken and stacked into a 3D composite image using ImageJ (Rasband, 1997–2015). To remove background fluorescence from the elastomer occurring in the DAPI (blue) channel, we performed an image based mathematical operation to subtract the auto fluorescent signal. This was accomplished using ImageJ's (Rasband, 1997–2015) "image calculator" function to subtract the known structure of the elastomer, defined by rhodamine staining, from the acquired DAPI channel data. Using this technique, the background fluorescence partially masking the cellular stain was adequately removed and permitted the clear visualization of DAPI stained nuclei distributed throughout the elastomer.

RESULTS

Synthesis

The as-synthesized, globular scaffolds are nematic main chain LCEs obtained from phenylbenzoate-based reactive nematic mesogens with photopolymerizable acrylate end-groups. All components (monomer, crosslinker, and photoinitiator) used for this report are commercially available and were prepared in an oil-in-water (toluene-in-H_2O) microemulsion using several surfactants including CTAB for comparison (Peinado et al., 2006), following a photopolymerization procedure reported earlier (Bera et al., 2015). Reactive mesogens are confined within organic droplets, and the photopolymerization reaction arrests the building blocks in the final globular structure (see **Figure 1**). Once the photopolymerization is complete, and the water–toluene solvent mixture is removed by evaporation, the final LCEs are thoroughly washed and rinsed to completely eliminate the surfactant, which results in voids between the LCE globules. Using this procedure, we selected the E20 formulation (toluene/H_2O = 80/20), which provides the best compromise between porosity and overall scaffold integrity, and replaced CTAB for several other surfactants. Of particular interest was the impact of these surfactants on the size and size distribution as well as on the surface morphology

(roughness) of the resulting LCE microspheres in comparison to the previously used CTAB.

Scaffold Characterization

All morphological studies were conducted using SEM. **Figure 2** shows that almost all of the tested surfactants using the E20 formulation facilitate the formation of globular LCE microstructures, but there are significant differences in the overall appearance. SDS and TritonX-100 give spherical microparticles fused together in the same way that the ones obtained using CTAB (**Figure 1**). The LCE microparticles formed using either SDS or TritonX-100 are about 30–40 μm in diameter with very smooth surfaces and almost perfectly defined individual microspheres (see inserts in **Figures 2A,B**). Both scaffolds are visibly porous with clearly discernable voids between the spheres (here, more so for TritonX-100). LCEs obtained with SDS are visually smoother and better defined that those obtained with TritonX-100. More importantly perhaps, the LCE microspheres obtained with the use of SDS are more homogeneous in size. The use of Brij C10 (which is chemically rather similar to TritonX-100), however, led to more "faceted" microspheres (i.e., quasi spherical irregular polyhedra), as reported for some of our previous formulations (Bera et al., 2015), and to smaller microspheres (~20 μm and smaller in diameter). In addition, BrijC10 leads to microspheres with a larger size polydispersity, and as a consequence, a lower level of porosity in comparison to the scaffold obtained with TritonX-100, because smaller microspheres fill in the voids. Nevertheless, the porosity is higher than for scaffolds synthesized in the presence of SDS and CTAB (**Figure 2C**). Finally, LCE microspheres obtained using CHAPS revealed less defined spherical shapes, making it almost impossible to recognize individual spheres. There is almost no contrast between the individual "spheres" with almost no voids between them, leading overall to the lowest porosity of scaffolds within the tested series of surfactants. CHAPS is based on cholesterol, and we assume that the tendency of the cholesterol moiety in CHAPS leads to significant mixing with the nematic reactive mesogens, practically reducing its ability to act as a true surfactant. Hence, the nature of the surfactant used has several effects on the morphology of the formed microspheres. Obtaining better defined more rounded morphologies may allow for higher internal porosity (larger voids) and permit cells to infiltrate through the bulk of the globular LCE constructs. Enhanced cell permeation within the LCE scaffold should facilitate cell growth and maturation. **Table 1** shows the values of the size and size distribution of the LCE microspheres and **Table 2** the values for the volume density (in %) and the pore

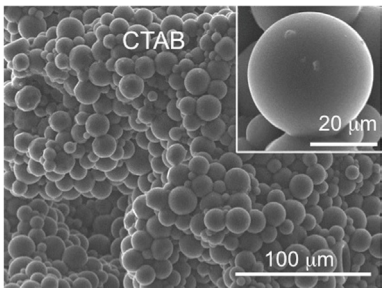

FIGURE 1 | Freeze fracture SEM image of globular LCE E20 obtained using CTAB as surfactant during microemulsion photopolymerization.

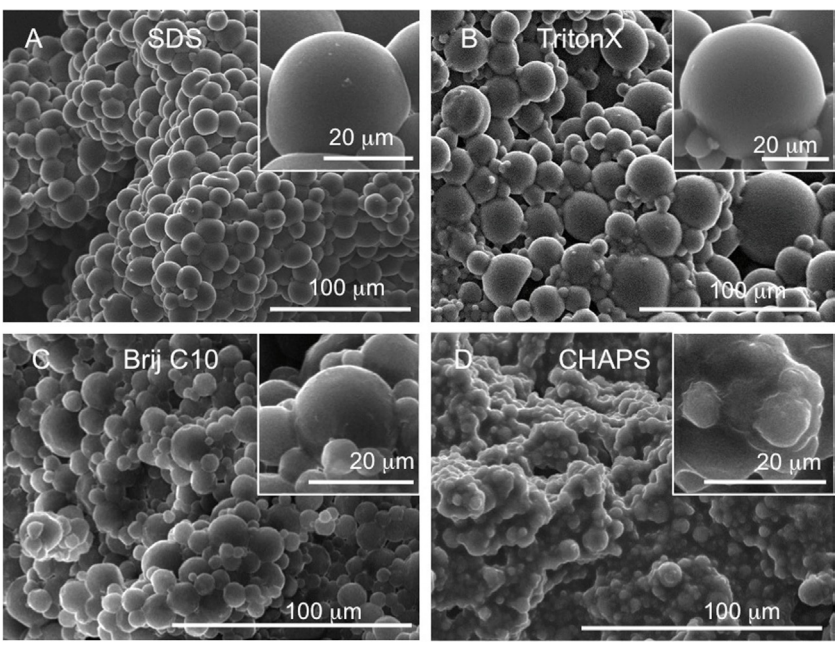

FIGURE 2 | Freeze fracture SEM images of globular LCE E20 prepared using different surfactants: (A) using SDS, (B) TritonX-100, (C) Brij C10, and (D) CHAPS.

TABLE 1 | Average size and size distribution of LCEs microspheres.

	Microsphere average size (μm)
SDS	15.6 ± 3.2
CTAB	13.3 ± 4.8
CHAPS	11.2 ± 7.3
TritonX-100	15.8 ± 8.7
Brij C10	17.3 ± 10.5

TABLE 2 | Volume density (%) and pore size diameter (micrometers) determined from SEM and/or confocal microscopy images of the microsphere scaffolds prepared in the presence of CTAB and SDS.

	Volume density (%)	Pore Size
		Diameter (μm)
SDS	42.6	66.8 ± 13.4
CTAB	38.0	77.5 ± 23.4

Volume density (%) was calculated as the % of the volume of elastomer that contained stained nuclei.

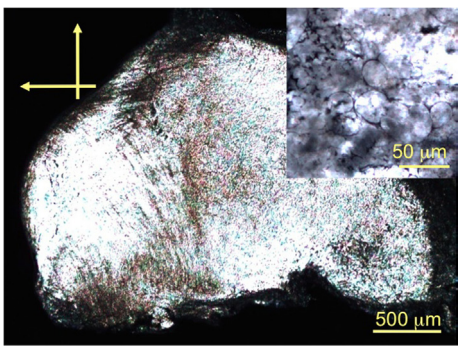

FIGURE 3 | POM photomicrographs (crossed polarizers) of the nematic LCE E20 taken at room temperature.

size diameter (in micrometer) of those microsphere scaffolds most extensively tested in cell studies.

Microemulsion photopolymerization using the different surfactants does not alter the chemical, thermal, or optical properties of the obtained LCEs. As we reported before, the phenylbenzoate-based LCEs form a nematic phase between 7 and 111°C (g 7 N 111 Iso). **Figure 3** shows the texture of the nematic phase (in principle the birefringence of the phase) of one of the scaffold samples. Compression leads to some loss of the spherical appearance (the sample is sandwiched between two glass slides), but the insert clearly shows the presence of the compressed microspheres.

Cell Studies

The use of CTAB for the preparation of globular LCEs was proven not to affect the viability of cells and allowed C2C12 cells to attach and proliferate for over 7 days (Bera et al., 2015). LCEs made with CTAB were tested to identify cytotoxic effects toward the cells; cells multiplied without any inherent cytotoxicity of the scaffolds in the absence of CTAB. To test the hypothesis that globular LCEs can also host other cells, we selected primary cells (hDF) and neuroblastomas (SHSY5Y) for this purpose. LCEs were briefly soaked in poly-D-lysine as a common treatment to promote cell adherence, temporarily masking the LCE's hydrophobic surfaces. Cells were seeded, and after 3 days we found that the cells adhered to the LCE scaffolds. Cells continued to grow, expanding throughout the bulk of the elastomer microsphere construct. **Figure 4** shows the 3D confocal microscopy images of DAPI stained nuclei of hDF (left) and SHSY5Y (right) attached to the rhodamine stained LCE at 10 days after cell seeding. Both types of SHSY5Y cells can be seen to have attached throughout the globular LCEs. It is of importance to note that hDF (primary) cells also appear to thrive within the matrix of the globular LCEs. The cell count for hDF as well as SHSY5Y at 10 days was found to be 17.54×10^3 and $16.30 \times 10^3/mm^3$, respectively. This represents a slight increase in comparison to the C2C12 at the same time point, which was found to be $12.23 \times 10^3/mm^3$ (Bera et al., 2015). The porosity of the LCEs made with CTAB, SDS, or TritonX-100 allows for better cell permeation within the elastomer construct, which would have not been possible for cells growing on LCEs made using CHAPS as surfactant.

To further analyze cellular attachment, samples of cellular development at several days after seeding were also analyzed using SEM. **Figure 5** shows cell attachment to the globular LCE scaffold construct (see **Figure 5A**ii and **Figure 5B**ii). Cells can also be seen to stretch across several microspheres underlining their expansion within the matrix. The SEM images show morphological phenotypes indicative of matured cells [as indicated by Teppola et al. (2016)]. Numerous neuritic extensions can be clearly seen in **Figure 5B**iii emanating from the cell body, resulting in the typical morphology of these cell types.

DISCUSSION

Liquid crystal elastomers have been proposed as artificial muscles, but only a very few unique examples of their biological use have been shown to date. The uniqueness of these types of LC-based cell scaffolds originates from their anisotropic response to external stimuli (such as temperature, elastic deformation, applied electric and magnetic fields) with an increase in ordering that can promote cell alignment and fusion in the absence of additional biological or chemical cues. The ease of synthetic structural variations that allows altering the hydrophilic–hydrophobic balance, tensile strength, biodegradation rate, and cell–scaffold interactions make LCEs ideal candidates for any type of cell study. The main properties that should be kept in mind during the selection of the components for LCE syntheses (monomers, cross-linkers) are that the obtained morphology and Young's moduli values should promote cell adhesion and extracellular matrix generation (ECM). The adhesive ligands of the ECM are critical for cell anchoring, and in some cases, it is also responsible for the acquisition of contractile phenotypes. Young's moduli values are important for cell adhesion, proliferation, and alignment prior to fusion into (for example) myotubes for C2C12s. Our data show that we can tune the porosity of nematic LCEs promoting cell adherence even when surfactants were used during synthesis. The globular morphologies described here provide porosity that

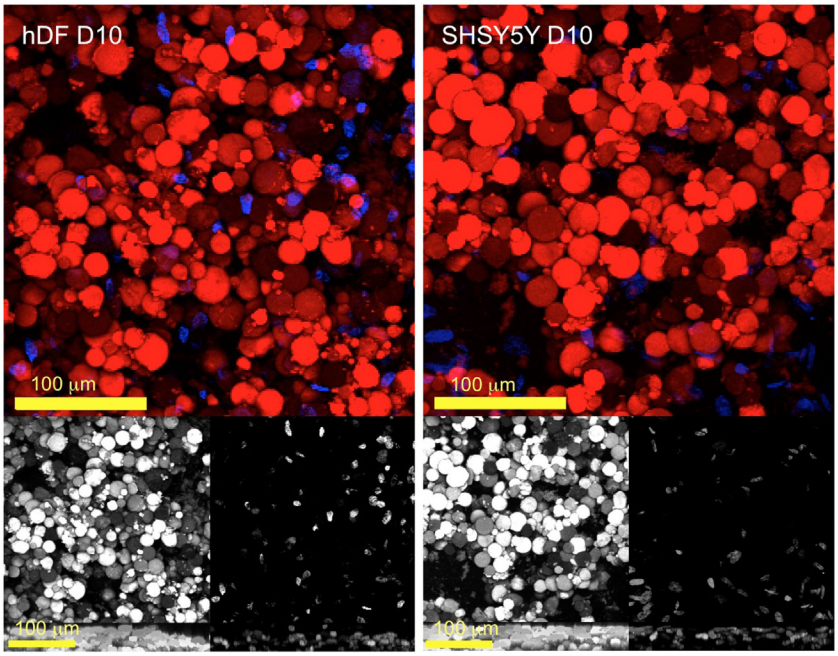

FIGURE 4 | Multi-channel confocal micrographs of hDF and SHSY5Y 10 days after seeding (on LCE E20) co-stained with rhodamine for the elastomer (red) and DAPI for cell nuclei (blue). The gray images in the lower panel represent the individual channels followed by a ZY projection to demonstrate the existence of multiple layers of cells distributed throughout the elastomer.

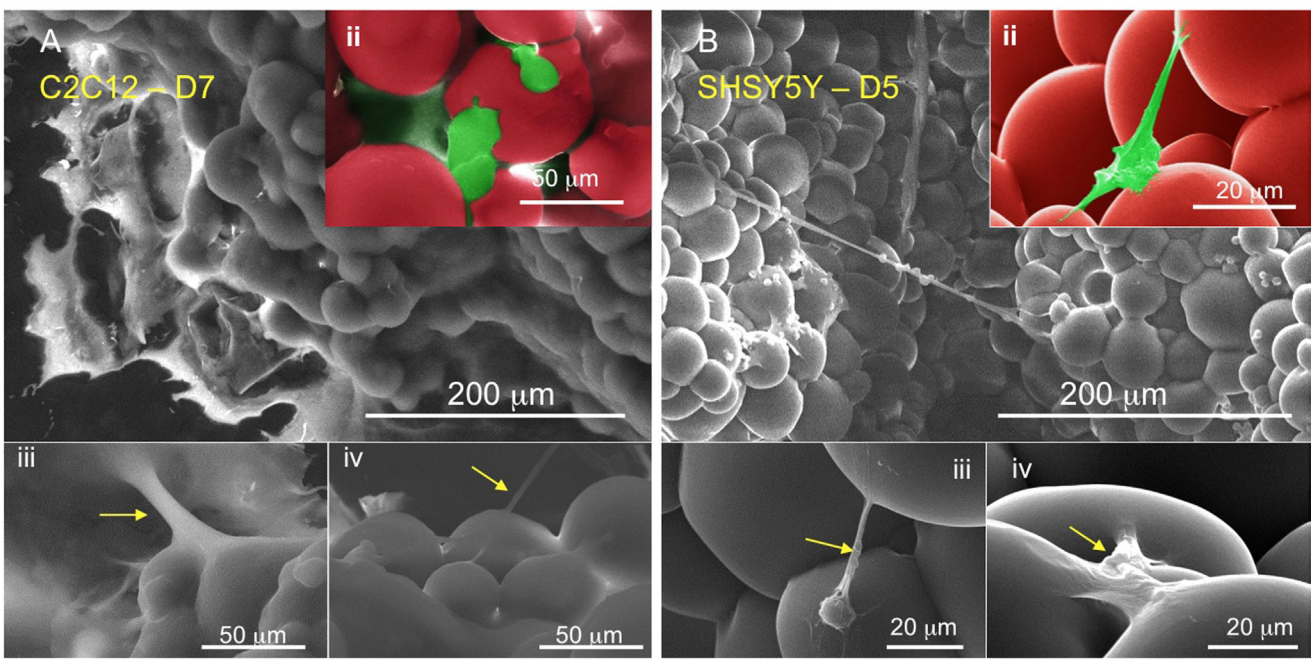

FIGURE 5 | Scanning electron micrographs of (A, ii–iv) C2C12 and (B, ii–iv) SHSY5Y after 7 and 5 days seeding, respectively. The cells (false colored green) can be seen as extending fibers directly attaching to the matrix for expansion and proliferation.

proved suitable for seeding, and growth of various cell lines. The ideal pore size for cell infiltration is usually around <30 μm [as found by Galperin et al. (2010)], characteristic of materials such as 3D layers of electrospun fibers. The porosity permits the cells to interact with their microenvironment while at the same time allowing for better mass transport (i.e., nutrients, gas, and

waste management). Since we can adjust porosity synthetically, as shown here simply by the choice of surfactant, the range of void volume can be tailored for specific cell microenvironments. Considering that we have previously shown that LCEs can host muscle cells, we moved into using other cell lines to further the scope of nematic LCEs for cell-related studies. Primary cell lines are difficult to grow; yet here, we have demonstrated a suitable scaffold for the growth of hDFs. Neuroblastomas are a common cell model for the study of neural diseases, and we found that they can also thrive on nematic LCE microsphere constructs. Furthermore, the cultured neurons grow in multiple layers dispersed throughout elastomer. The distribution throughout the globular support matrix permits neurons to spatially differentiate mimicking endogenous neural environments. These qualities of the LCE matrix support their use as a platform to recapitulate the native architecture and discrete cellular components of human tissue for long-term cell cultures as well as the next generation of smart tissue implants. Ongoing studies in our groups are on the continuous use of LCEs to test stimulus pathways to trigger cell alignment, ECM formation, and in some cases differentiation to particular cell lines.

CONCLUSION

We have previously demonstrated that nematic globular-LCE scaffolds allow for attachment, growth, and proliferation of skeletal muscle cells (C2C12 myoblasts, Bera et al., 2015). In this follow-up study, we demonstrate that other surfactants not only promote globular LCE scaffold formation, allowing us to tune several morphological parameters that ultimately allow for the multiplication of even challenging cell lines. The use of CTAB in any cell or biological study has always been controversial. While we previously showed that no traces of CTAB remained in the matrix allowing for the growth and expansion of C2C12 cells, it was necessary to study the effect of other surfactants on the final morphology of these LCE microsphere scaffolds and study cell attachment and proliferation. We have expanded the use of globular morphologies to different cell lines and showed that they attach and thrive. We also evaluate cell structure and verified morphological phenotypes indicative of normal, healthy, and developed cells as reported in the literature (Teppola et al., 2016). The use of less toxic surfactants in this study further encourages studies into globular LCE scaffolds that can support cell growth and be used without the concern of the surfactants' inherent toxicity. Further studies now aim at longitudinal cell studies using these 3D spatial cell scaffolds, where the liquid crystalline properties (nematic phase, in this case, and smectic phases in others) are studied and exploited to promote cell proliferation and particularly cell alignment.

AUTHOR CONTRIBUTIONS

The manuscript was written through contributions of all authors. EH, research idea, all data analysis and writing of the manuscript with important contributions from RC and CM. EH, CM, and RC were PIs on the project. TB prepared LCEs, performed confocal and cell culture, and pre-analyzed SEM and confocal images. RC analyzed all confocal. All authors have given approval to the final version of the manuscript.

ACKNOWLEDGMENTS

Authors thank KSU for financial support of the Regenerative Medicine Initiative at Kent State University (ReMedIKS) and undergraduate students Karene Diabre and Brittany Barnard are acknowledged for their help in cell culture studies of LCEs. All authors thank Torsten Hegmann for his leadership and directing the ReMedIKS effort.

REFERENCES

Abbott, N. L., de Pablo, J. J., Palecek, S. P., Lockwood, N. A., Mohr, J. C., Murphy, C. J., et al. (2010). *Liquid Crystalline Substrates for Culturing Cells*. U.S. Patent 7,732,152.

Alge, D. A., Azagarsamy, M. A., Donohue, D. F., and Anseth, K. S. (2013). Synthetically tractable click hydrogels for three-dimensional cell culture formed using tetrazine-norbornene chemistry. *Biomacromolecules* 8, 949–953. doi:10.1021/bm4000508

Bera, T., Freeman, E. J., McDonough, J. A., Clements, R. J., Aladlaan, A., Miller, D. W., et al. (2015). Artificial muscles as cell scaffolds: nematic liquid crystal elastomers supporting the attachment and proliferation of myoblasts. *ACS Appl. Mater. Interfaces* 7, 14528–14535. doi:10.1021/acsami.5b04208

Buguin, A., Li, M. H., Silberzan, P., Ladoux, B., and Keller, P. (2006). Micro-actuators: when artificial muscles made of nematic liquid crystal elastomers meet soft lithography. *J. Am. Chem. Soc.* 128, 1088–1089. doi:10.1021/ja0575070

Chargè, S. P. B., and Rudnicki, M. A. (2004). Cellular and molecular regulation of muscle regeneration. *Physiol. Rev.* 84, 209–238. doi:10.1152/physrev.00019.2003

De Gennes, P.-G. (1997). A semi-fast artificial muscle. *C. R. Acad. Sci. Paris Ser. IIB* 324, 343–348.

De Gennes, P. G., Hebert, M., and Kant, R. (1997). Artificial muscles based on nematic gels. *Macromol. Symp.* 113, 39–49. doi:10.1002/masy.19971130107

DeForest, C. A., and Anseth, K. S. (2012). Bioactive hydrogels for regenerative medicine. *Annu. Rev. Chem. Biomol. Eng.* 3, 421–444. doi:10.1146/annurev-chembioeng-062011-080945

Discher, D. E., Mooney, D. J., and Zandstra, P. W. (2009). Growth factors, matrices, and forces combine and control stem cells. *Science* 324, 1673–1677. doi:10.1126/science.1171643

Engler, A. J., Sen, S., Sweeney, H. L., and Discher, D. E. (2006). Matrix elasticity directs stem cell lineage specification. *Cell* 126, 677–689. doi:10.1016/j.cell.2006.06.044

Fang, J., Ma, W., Selinger, J. V., and Shashidhar, R. (2003). Imaging biological cells using liquid crystals. *Langmuir* 19, 2865–2869. doi:10.1021/la0264062

Finkelmann, H., and Shahinpoor, M. (2002). Electrically-controllable liquid crystal elastomer-graphite composite artificial muscles. *Proc. SPIE* 4695, 459–464. doi:10.1117/12.475190

Fleischmann, E. K., and Zentel, R. (2013). Liquid-crystalline ordering as a concept in materials science: from semiconductors to stimuli-responsive devices. *Angew. Chem. Int. Ed. Engl.* 52, 8810–8827. doi:10.1002/anie.201300371

Galperin, A., Long, T. J., and Ratner, B. D. (2010). Degradable, thermo-sensitive poly(*n*-isopropyl acrylamide)-based scaffolds with controlled porosity for tissue engineering applications. *Biomacromolecules* 11, 2583–2592. doi:10.1021/bm100521x

Gao, Y., Manning, S., Zhao, Y., Nielsen, A. D., Mori, T., Neshat, A., et al. (2016). Biocompatible 3D liquid crystal elastomer cell scaffolds and foams with primary and secondary porous architecture. *ACS Macro Lett.* 5, 4–9. doi:10.1021/acsmacrolett.5b00729

Gilbert, P. M., Havenstrite, K. L., Magnusson, K. E. G., Sacco, A., Leonardi, N. A., Kraft, P., et al. (2010). Substrate elasticity regulates skeletal muscle stem cell self-renewal in culture. *Science* 329, 1078–1081. doi:10.1126/science.1191035

Harris, K. D., Cuypers, R., Scheibe, P., van Oosten, C. L., Bastiaansen, C. W. M., Lub, J., et al. (2005). Large amplitude light-induced motion in high elastic modulus polymer actuators. *J. Mater. Chem.* 15, 5043–5048. doi:10.1039/b512655j

Haseloh, S., Ohm, C., Smallwood, F., and Zentel, R. (2011). Nanosized shape-changing colloids from liquid crystalline elastomers. *Macromol. Rapid Commun.* 32, 88–93. doi:10.1002/marc.201000324

Haseloh, S., van der Schoot, P., and Zentel, R. (2010). Control of mesogen configuration in colloids of liquid crystalline polymers. *Soft Matter* 6, 4112–4119. doi:10.1039/c0sm00125b

Koegler, W. S., and Griffith, L. G. (2004). Osteoblast response to PLGA tissue engineering scaffolds with PEO modified surface chemistries and demonstration of patterned cell response. *Biomaterials* 25, 2819–2830. doi:10.1016/j.biomaterials.2003.09.064

Kotov, N. A., Liu, Y. F., Wang, S. P., Cumming, C., Eghtedari, M., Vargas, G., et al. (2004). Inverted colloidal crystals as three-dimensional cell scaffolds. *Langmuir* 20, 7887–7892. doi:10.1021/la049958o

Lange, B., Metz, N., Tahir, M. N., Fleischhaker, F., Theato, P., Schroder, H. C., et al. (2007). Functional polymer-opals from core-shell colloids. *Macromol. Rapid Commun.* 28, 1987–1994. doi:10.1002/marc.200700284

Lee, J., and Kotov, N. A. (2009). Notch ligand presenting a cellular 3D microenvironments for ex vivo human hematopoietic stem-cell culture made by layer-by-layer assembly. *Small* 5, 1008–1013. doi:10.1002/smll.200801242

Lee, J., Lilly, G. D., Doty, R. C., Podsiadlo, P., and Kotov, N. A. (2009). In vitro toxicity testing of nanoparticles in 3d cell culture. *Small* 5, 1213–1221. doi:10.1002/smll.200801788

Lewis, K. J. R., and Anseth, K. S. (2013). Hydrogel scaffolds to study cell biology in four dimensions. *MRS Bull.* 38, 260–268. doi:10.1557/mrs.2013.54

Li, M. H., and Keller, P. (2006). Artificial muscles based on liquid crystal elastomers. *Philos. Trans. A Math. Phys. Eng. Sci.* 364, 2763–2777. doi:10.1098/rsta.2006.1853

Liu, Y. F., Wang, S. P., Lee, J. W., and Kotov, N. A. (2005). A floating self-assembly route to colloidal crystal templates for 3D cell scaffolds. *Chem. Mater.* 17, 4918–4924. doi:10.1021/cm048050g

Lockwood, N. A., Mohr, J. C., Ji, L., Murphy, C. J., Palecek, S. P., de Pablo, J. J., et al. (2006). Thermotropic liquid crystals as substrates for imaging the reorganization of matrigel by human embryonic stem cells. *Adv. Funct. Mater.* 16, 618–624. doi:10.1002/adfm.200690018

Lowe, A. M., and Abbott, N. L. (2012). Liquid crystalline materials for biological applications. *Chem. Mater.* 24, 746–758. doi:10.1021/cm202632m

Lub, J., Broer, D. J., Wegh, R. T., Peeters, E., and van der Zande, B. M. I. (2005). Formation of optical films by photo-polymerisation of liquid crystalline acrylates and application of these films in liquid crystal display technology. *Mol. Cryst. Liq. Cryst.* 429, 77–99. doi:10.1080/15421400590930773

Marshall, J. E., Gallagher, S., Terentjev, E. M., and Smoukov, S. K. (2014). Anisotropic colloidal micromuscles from liquid crystal elastomers. *J. Am. Chem. Soc.* 136, 474–479. doi:10.1021/ja410930g

Mayer, S., and Zentel, R. (2002). Liquid crystalline polymers and elastomers. *Curr. Opin. Solid State Mater. Sci.* 6, 545–551. doi:10.1016/S1359-0286(03)00011-1

McCall, J. D., Luoma, J. E., and Anseth, K. S. (2012). Covalently tethered transforming growth factor beta in PEG hydrogels promotes chondrogenic differentiation of encapsulated human mesenchymal stem cells. *Drug Deliv. Transl. Res.* 2, 305–312. doi:10.1007/s13346-012-0090-2

McKinnon, D. D., Kloxin, A. M., and Anseth, K. S. (2013). Synthetic hydrogel platform for three-dimensional culture of embryonic stem cell-derived motor neurons. *Biomater. Sci.* 1, 460–469. doi:10.1039/c3bm00166k

Pei, Z. Q., Yang, Y., Chen, Q. M., Terentjev, E. M., Wei, Y., and Ji, Y. (2014). Mouldable liquid-crystalline elastomer actuators with exchangeable covalent bonds. *Nat. Mater.* 13, 36–41. doi:10.1038/nmat3812

Peinado, C., Bosch, P., Martin, V., and Corrales, T. (2006). Photoinitiated polymerization in bicontinuous microemulsions: fluorescence monitoring. *J. Polym. Sci. Polym. Chem.* 44, 5291–5303. doi:10.1002/pola.21649

Rasband, W. S. (1997–2015). *ImageJ*. Bethesda, MD: U.S. National Institutes of Health. Available at: http://imagej.nih.gov/ij/

Ratna, B. R., Thomsen, D. L., and Keller, P. (2001). Liquid crystal elastomers as artificial muscles: role of side-chain-backbone coupling. *Proc. SPIE* 4329, 233–237. doi:10.1117/12.432651

Shanbhag, S., Wang, S. P., and Kotov, N. A. (2005). Cell distribution profiles in three-dimensional scaffolds with inverted-colloidal-crystal geometry: modeling and experimental investigations. *Small* 1, 1208–1214. doi:10.1002/smll.200500191

Sharma, A., Neshat, A., Mahnen, C. J., Nielsen, A. D., Snyder, J., Stankovich, T. L., et al. (2014). Biocompatible, biodegradable and porous liquid crystal elastomer scaffolds for spatial cell cultures. *Macromol. Biosci.* 15, 200–214. doi:10.1002/mabi.201400325

Shi, X., and Garry, D. J. (2006). Muscle stem cells in development, regeneration, and disease. *Genes Dev.* 20, 1692–1708. doi:10.1101/gad.1419406

Teppola, H., Sarkanen, J. R., Jalonen, T. O., and Linne, M. L. (2016). Morphological differentiation towards neuronal phenotype of SH-SY5Y neuroblastoma cells by estradiol, retinoic acid and cholesterol. *Neurochem. Res.* 41, 731–747. doi:10.1007/s11064-015-1743-6

Thomsen, D. L., Keller, P., Naciri, J., Pink, R., Jeon, H., Shenoy, D., et al. (2001). Liquid crystal elastomers with mechanical properties of a muscle. *Macromolecules* 34, 5868–5875. doi:10.1021/ma001639q

Vennes, M., Zentel, R., Rossle, M., Stepputat, M., and Kolb, U. (2005). Smectic liquid-crystalline colloids by miniemulsion techniques. *Adv. Mater.* 17, 2123–2127. doi:10.1002/adma.200500310

Zammit, P. S., Partridge, T. A., and Yablonka-Reuveni, Z. (2006). The skeletal muscle satellite cell: the stem cell that came in from the cold. *J. Histochem. Cytochem.* 54, 1177. doi:10.1369/jhc.6R6995.2006

Conflict of Interest Statement: The authors declare that the research was conducted in the absence of any commercial or financial relationships that could be construed as a potential conflict of interest.